World Academy of Science, Engineering and Technology
International Journal of Mechanical and Mechatronics Engineering
Vol:10, No:7, 2016

Numerical Simulations of Electronic Cooling with In-Line and Staggered Pin Fin Heat Sinks

Yue-Tzu Yang, Hsiang-Wen Tang, Jian-Zhang Yin, Chao-Han Wu

Abstract**—**Three-dimensional incompressible turbulent fluid flow and heat transfer of pin fin heat sinks using air as a cooling fluid are numerically studied in this study. Two different kinds of pin fins are compared in the thermal performance, including circular and square cross sections, both are in-line and staggered arrangements. The turbulent governing equations are solved using a control-volume-based finite-difference method. Subsequently, numerical computations are performed with the realizable k - ε turbulence for the parameters studied, the fin height H, fin diameter D, and Reynolds number (Re) in the range of $7 \le H \le 10$, $0.75 \le D \le 2$, $2000 \le \mathrm{Re} \le 126000$ respectively. The numerical results are validated with available experimental data in the literature and good agreement has been found. It indicates that circular pin fins are streamlined in comparing with the square pin fins, the pressure drop is small than that of square pin fins, and heat transfer is not as good as the square pin fins. The thermal performance of the staggered pin fins is better than that of in-line pin fins because the staggered arrangements produce large disturbance. Both in-line and staggered arrangements show the same behavior for thermal resistance, pressure drop, and the entropy generation.

Keywords**—**Pin-fin, heat sinks, simulations, turbulent flow.

I. Introduction

PIN fins as elements for heat transfer enhancement have been investigated by numerous researchers. The pin fins increase not only the internal wetted (cooled) surface area, but also the structure integrity and stiffness. On the other hand, when the fluid flows across the pin fin arrays, the pin fins create accelerated flow between pins, and produce highly disturbed wake regions behind each pin, horseshoe vortices from interaction with the end wall, and unsteady vertical shedding induced from the pin. These mechanisms served to produce a high turbulence level in the flow and significantly enhanced the convective heat transfer performance. Basic research on heat transfer and pressure drop characteristics was performed by [1]-[3]. Hence, [4] and [5] investigated the relative merits of pin fin heat transfer and end wall heat transfer in the overall pin array heat transfer. Despite the previous contributions regarding different cross-sections of pin fins, it was still not clear which pin cross-section would give the best results for a given geometry of the channel. This confusion was due to different flow rates used in the experiments and to different styles of data presentation. Furthermore, the experiments were carried out for different span-wise and flow direction spaces, different pin lengths, different pin rows and for different tip clearances. The different performance evolution criteria used for the assessment of the performance of their investigated pin arrays made the comparison of the investigated pin fin arrays even more complicated. In order to avoid the above-mentioned difficulties in the performance comparison but still to include various possible configurations, two geometric criteria for comparison were selected: the first basically allowed comparisons under similar fluid dynamic and thermal conditions whereas the second included the geometric similarity derived from the point of view of practical applications. In order to derive an appropriate computational model, the thermal and fluid dynamic characteristics of the flow over pin fin arrays have to be considered. Whereas the heat transfer in the cross-flow over a pin array was a typical example of external convective heat transfer, the flow through a channel containing pins has characteristics of internal flows. As in the fluid flow across the pins no thick thermal boundary layer can be built, the heat transfer is usually higher than the other fin geometries. Flow over pin fins, particularly over pin fins with high ratios of pin length to pin diameter, resembled very much the flow over tube banks. As in the application of tube banks, staggered and in-line pin fin arrays were more common. Similarly, to the flow over tube banks, the characteristics of the flow with heat transfer through pin arrays depended basically on transversal and longitudinal center-to-center pin distances and the inlet fluid flow velocity. Observations made by different workers for the flow regime over tube banks should be taken with proviso for the assessment of the flow regime over pin fins. This is because side walls have a considerable influence on the basic friction and heat transfer characteristics. Hence the side wall effect in arrays comprising pin fins cannot be neglected. The friction on the side wall changes the fluid dynamic patterns of the flow regime, which may differ from those observed in tube banks. Such walls in the tube bank models are much far from each other and hence the tubes are usually considered to be infinitely long, as the influence of side walls on the heat transfer and pressure drop coefficients is minor. In the present computation, the friction on the side walls additionally influences the flow field, resulting in complicated 3D vortices. In order to provide a fair and physically meaningful basis for the comparison, appropriate geometric comparison criteria which provide similar model dimensions have to be selected. Furthermore, the thermal conditions and fluid properties have to be similar in order to assess the relative

Y. T. Yang is with the Department of Mechanical Engineering, National Cheng Kung University, Tainan 70101, Taiwan. (phone: +886-6-2757575x62172; fax: +886-6-2352973; e-mail: ytyang@mail.ncku.edu.tw).

Hsiang-Wen Tang, Jian-Zhang Yin, and Chao-Han Wu were with the Department of Mechanical Engineering, National Cheng Kung University, Tainan 70101, Taiwan.

advantages of different pin fin cross-section. Hence two different geometric criteria were employed.

Won et al. [6] and Ames et al. [7] studied the local Nusselt number and turbulent flow structure characteristics in a pin fin channel, and their study revealed that the unsteadiness in the wakes, the shear layers formed between the wake and the high speed mainstream flow, and the horseshoe vortices formed near the pin fins, increase mixing and turbulent transport in the pin fin channel, which is responsible for the heat transfer enhancement. Lyall et al. [8] studied the effects of the transverse spacing on the local heat transfer from a row of pin fins, and indicated that a smaller transverse spacing of pin fins results in higher end wall heat transfer due to strong interaction between the wakes. Kondo et al. [9] considered two types of heat sink: plate fins and pin-fins. They optimized the heat sink geometry by evaluating sixteen parameters simultaneously. For the plate fins, the optimal thickness was found to be 0.12- 0.15 mm. For the pin-fins, optimal pin diameters were 0.39- 0.40 mm. Under the conditions of constant pumping power, the optimal thermal resistance of the plate fins was about 60 % of the pin-fins. An experimental and modeling study performed by Dogruoz et al. [10] on square, in-line pin-fin heat sinks to measure the overall thermal resistance as a function of Reynolds number and bypass height and identify optimum pin spacing as a function of clearance ratio. Entropy generation minimization (EGM) procedure was used to optimize the overall performance of pin-fin heat sinks [11]. They showed that the entropy generation rate depends on two main performance parameters, i.e. thermal resistance and pressure drop, which in turn depend on the average heat transfer and friction coefficients. Recently, [12] numerically studied perforated fins, which performed better and weighed less than solid fins.

Kosar and Peles [13] compared the hydrodynamic and thermal performances of micro pin-fin heat sinks having circular, rectangular, hydrofoil, and cone-shaped micro pin-fins. The study concluded that the denser pin-fin configuration has better performance at high Re values, and the more sparsely packed pin-fin configuration was better at low Re values. The best thermal performance at low Re values (Re < 40) was observed with the rectangular pin-fin configuration. John et al. [14] investigated the effect of pin-fin geometry for square and circular micro pin-fins. They observed that the circular pin-fins had better performance compared to the square pin-fins at *Re* values below 300, while the square pin-fins had better performance compared to the circular pin-fins at higher *Re* values. Tullius et al. [15], [16] compared the thermal performances of micro pin-fin heat sinks having circle, square, triangle, ellipse, diamond-shaped, and hexagon-shaped micro pin-fins in a staggered array, where these are attached to the bottom heated surface of a rectangular mini-channel. Effects of fin height, width, spacing, and material were investigated, and the best performance was observed with triangular pin-fins with larger fin height and smaller fin width.

Türker et al. [17] performed the evaluation study by using three-dimensional (3D) numerical models in the light of flow morphologies around micro pin-fins of various shapes. According to the results obtained from their study, the rectangular-shaped micro pin-fin configuration has the highest Nusselt number and friction factor over the whole Reynolds number range. Heat transfer and pressure drop characteristics of a set of pin-fins with uniform heat flux were investigated experimentally and numerically by [18]. It was designed to assess the effects of mass flow rate, fin height, and fin density on convection heat transfer and pressure drop. The flow field of various design parameters of the heat sink was simulated. It was found that heat sinks having fin heights of 20 and 30 mm operated at a lower Reynolds number reached minimum value for thermal resistance when the fin density 10×10.

The reliable computational fluid dynamics (CFD) simulations of various constructal pin-fin models were performed by [19], and the detailed flow and heat transfer characteristics were presented. The results showed that by using the proposed system with optimized pin-fin heat exchanger the stored thermal energy can be increased by 10.2%. Horiuchi et al. [20] presented the multi-objective optimization of water-cooled pin fin heat sinks. The heat transfer rate and pressure drop were the objective functions, and four parameters (height, diameter, longitudinal pitch, and transverse pitch) of pin fin geometry were the design variables. They showed that small clearance caused the reduction of pressure drop while maintaining high heat transfer performance.

It can be seen that although heat transfer characteristics in pin fin channels has been thoroughly investigated from the above literature mentioned. Very few studies the turbulent flow both thermal and hydraulic resistances simultaneously. In this study, numerical computations are performed with the realizable $k-\varepsilon$ turbulence for the parameters studied for in-line and staggered pin fin heat sinks.

II. Mathematical Formulation

The schematic diagram of the geometry and the computational domain is shown in Fig. 1. The turbulent three-dimensional Navier-Stokes and energy equations are solved numerically by a control-volume-based finite-difference method to simulate the thermal and turbulent flow fields. The following assumptions are used to simulate the in-line and staggered pin-fin heat sink.

(1) Three-dimensional turbulent flow
(2) Steady state
(3) Incompressible fluid
(4) Constant fluid properties
(5) Negligible radiative heat transfer

A. Governing Equations

To describe the conjugate heat transfer, the continuity, momentum and energy equations are required. With the assumptions described above and the governing equations are as:

- Continuity equation:

$$\frac{\partial \overline{u}_i}{\partial x_i} = 0 \tag{1}$$

- Momentum equation:

$$\rho \overline{u}_j \frac{\partial \overline{u}_i}{\partial x_i} = -\frac{\partial \overline{P}}{\partial x_i} + \frac{\partial}{\partial x_j}\left[\mu_l\left(\frac{\partial \overline{u}_i}{\partial x_j} + \frac{\partial \overline{u}_j}{\partial x_i}\right) - \rho\overline{u_i u_j}\right] \tag{2}$$

- Energy equation for fluid cells:

$$\rho \overline{u}_j \frac{\partial \overline{T}}{\partial x_j} = \frac{\partial}{\partial x_j}\left[\left(\frac{\mu_l}{\sigma_l} + \frac{\mu_t}{\sigma_t}\right)\frac{\partial \overline{T}}{\partial x_j}\right] \tag{3}$$

- Energy equation for solid cells:

$$\frac{\partial}{\partial x_i}\left(k_s \frac{\partial T}{\partial x_i}\right) = 0 \tag{4}$$

B. Turbulence Models

Present study compares four different turbulence models to verify the difference with experimental data. Four models are Standard $k-\varepsilon$ model, RNG $k-\varepsilon$ model, Realizable $k-\varepsilon$ model and Reynolds stress model. From present results, the realizable $k-\varepsilon$ model shows the better results in comparing with the experimental data. Therefore, the following numerical computations are presented by using the standard $k-\varepsilon$ model. The transport equations for *k* and ε are given as:

- Transport equation for *k:*

$$\rho \overline{u}_j \frac{\partial k}{\partial x_i} = \frac{\partial}{\partial x_j}\left[\left(\mu_l + \frac{\mu_t}{\sigma_k}\right)\frac{\partial k}{\partial x_j}\right] + \mu_t\left(\frac{\partial \overline{u}_i}{\partial x_j} + \frac{\partial \overline{u}_j}{\partial x_i}\right)\frac{\partial \overline{u}_i}{\partial x_j} - \rho\varepsilon \tag{5}$$

- Transport equation for ε *:*

$$\rho \overline{u}_j \frac{\partial \varepsilon}{\partial x_j} = \frac{\partial}{\partial x_j}\left[\left(\mu_l + \frac{\mu_t}{\sigma_\varepsilon}\right)\frac{\partial \varepsilon}{\partial x_j}\right] + C_1\mu_t\frac{\varepsilon}{k}\left(\frac{\partial \overline{u}_i}{\partial x_j} + \frac{\partial \overline{u}_j}{\partial x_i}\right)\frac{\partial \overline{u}_i}{\partial x_j} - C_2\rho\frac{\varepsilon^2}{k+\sqrt{\nu\varepsilon}} \tag{6}$$

where,

$$\mu_t = \rho C_\mu \frac{k^2}{\varepsilon} \tag{7}$$

The closures coefficients appear in the above equations are given by the following values:

$$C_1 = 1.44, C_2 = 1.92, C_\mu = 0.09, \sigma_k = 1.0, \sigma_\varepsilon = 1.3$$

C. Boundary Conditions

Fig. 1 shows the settings of boundary conditions on each boundary of the computational domain. The boundary conditions in this study can be summarized as follows:

(1) Inlet boundary

$$u = u_{in},\ v = w = 0$$

$$\mathrm{T} = T_{in} = 293K \tag{9}$$

$$k_{in} = \frac{2}{3}\left(Iu_{in}\right)^2 \tag{10}$$

$$\varepsilon_{in} = C_\mu^{3/4}\frac{k_{in}^{3/2}}{D_h} \tag{11}$$

(2) Outlet boundary

$$P = 1atm \tag{12}$$

$$\frac{\partial k}{\partial x} = \frac{\partial \varepsilon}{\partial x} = \frac{\partial T_f}{\partial x} = 0 \tag{13}$$

(3) Bottom heated wall boundary

$$q" = 3094W/m^2 \tag{14}$$

(4) Symmetry boundary

$$\frac{\partial k}{\partial y} = \frac{\partial \varepsilon}{\partial y} = \frac{\partial u}{\partial y} = \frac{\partial w}{\partial y} = \mathrm{v} = \frac{\partial T_f}{\partial y} = 0 \tag{15}$$

(5) Conjugate boundary

$$\mathrm{u} = \mathrm{v} = \mathrm{w} = 0,\ T_s = T_f, k_s\frac{\partial T_s}{\partial n} = k_f\frac{\partial T_f}{\partial n} \tag{16}$$

III. Numerical Calculations and Validations

A. Grid Independence Check

The numerical computations are carried out by solving the governing conservation equations with the boundary conditions. This study chooses the non-uniform meshes to build the grid system. The solution procedure is based on SIMPLE algorithm. The convection term of governing conservation equations is discretized by a control volume based finite difference method with a QUICK scheme. A set of different equations is solved iteratively using a line by line solution method in conjunction with a matrix form. The solution is considered to converge when the normalized residual of the algebraic equation is less than a prescribed value of 10^{-4}. In the present study, three different grid numbers are chosen to validate the grid dependence of each case. The variations in thermal resistance with Re at different grid numbers has been shown in Fig. 2. The figure shows that the numerical results and the reference experimental data [21] of thermal resistance are quite close. And the results show that the difference of thermal resistance between the case of very fine and the fine numbers of grid are less than 3%. Therefore, the fine numbers of grid are chosen to carry out the calculations in the present study.

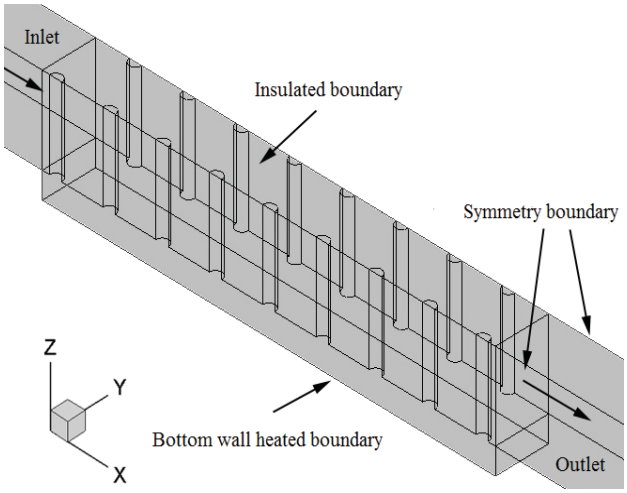

(a)

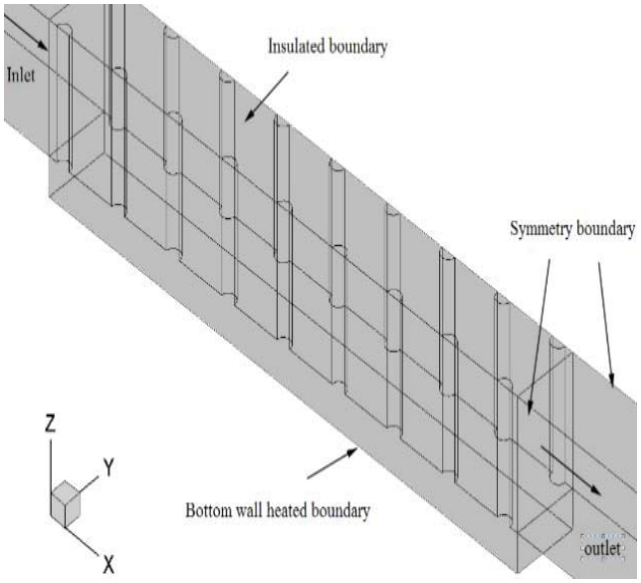

(b)

Fig. 1 Schematic diagram and boundary conditions of (a) staggered (b) in-line pin fin heat sink

B. Validations of Turbulence Model

To find an appropriate turbulence model to predict the flow fields, three different turbulence model, standard $k-\varepsilon$ model, RNG $k-\varepsilon$ model and realizable $k-\varepsilon$ model are chosen to compare with the experimental data which was published by [21]. The variations of thermal resistance with Reynolds number at three different turbulence models are shown in Fig. 3. It can be seen that the results which is predicted by realizable $k-\varepsilon$ model and the reference experimental data are quite close for the in-line and staggered circular pin fin heat sinks. Therefore, realizable $k-\varepsilon$ model was chosen to predict this turbulent flow fields in the present study.

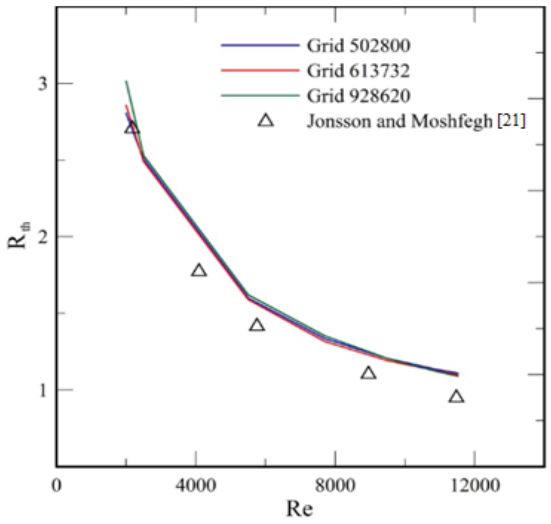

(a)

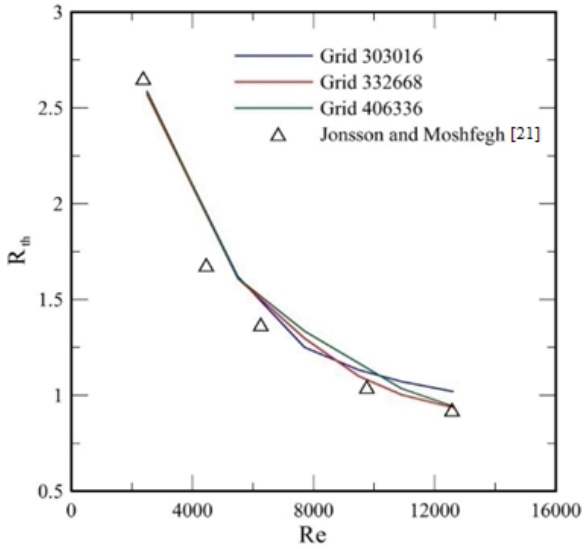

(b)

Fig. 2 Grid independence check for (a) in-line (b) staggered circular pin fin heat sink

IV. Results and Discussion

The temperature distributions of staggered and in-line circular pin fin heat sink are shown in Fig. 4. It can be seen that thermal boundary layer thickness near the upstream is thinner than that near the downstream. Therefore, the conduction heat transfer rate on the wall near the upstream is higher than that near the downstream. It is worth to noting that the boundary layer thickness near the outlet of the in-line square pin fin heat sink channel is thinner than that of the staggered case because the fluctuations in the flow field of the staggered case are stronger than that of the in-line case.

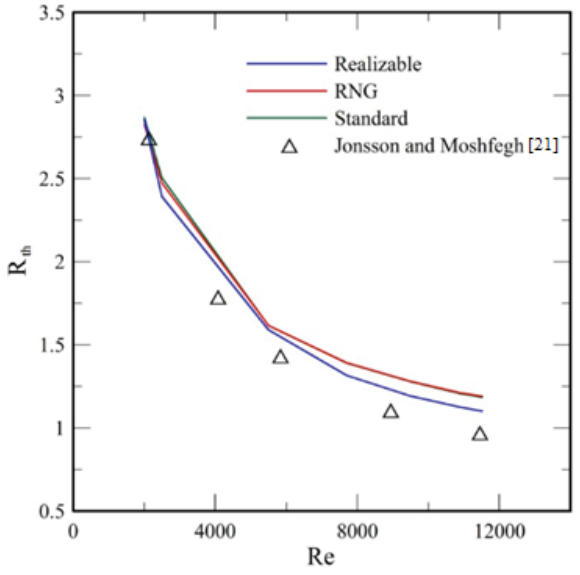

(a)

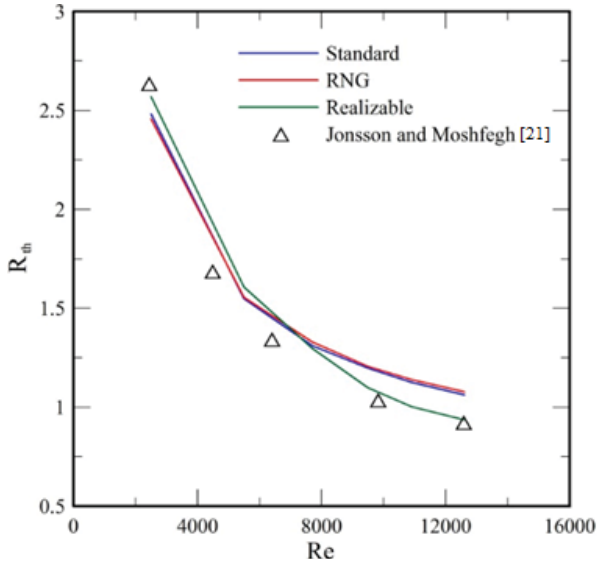

(b)

Fig. 3 Thermal resistance variations with Re for different turbulence models for (a) in-line circular (b) staggered square pin fin heat sink

Fig. 5 shows that the variations in average Nusselt numbers with Reynolds number of square pin fin heat sink. It can be seen that the average Nusselt number of staggered and in-line case are significantly higher than that of without pin fin case. It is because the presence of pin fin increases the total heat transfer area in the channel. Otherwise, the average Nusselt number of staggered case is slightly higher than that of in-line case. It is because the stronger fluctuations in the channel of staggered case than that in the channel of in-line case may enhance the mixing of fluid in the channel.

Fig. 6 shows that the variations in average Nusselt numbers with Reynolds number of circular pin fin heat sink. Similar to Fig. 5, the difference of average Nusselt number between pin fin case and without pin fin case is because of the difference of total heat transfer area in the channel. And the average Nusselt numbers of in-line case is higher than that of staggered case when Re > 8000, but it is very close to that of staggered case when Re < 8000.

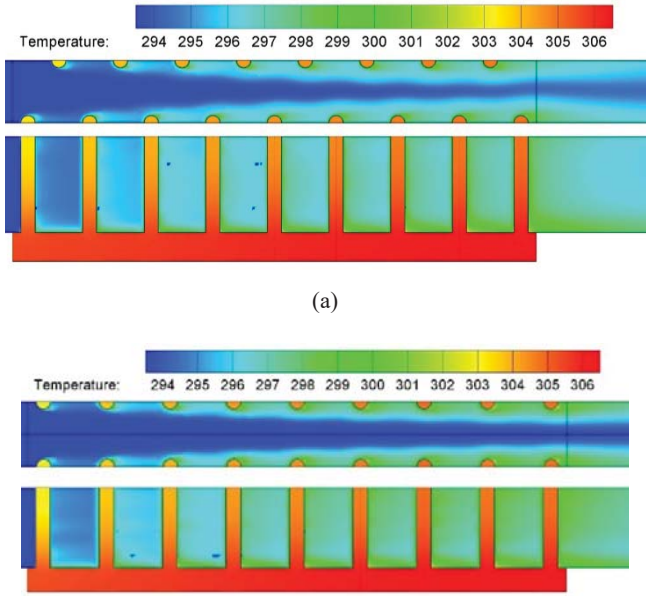

(a)

(b)

Fig. 4 Temperature contours of (a) staggered (b) in-line circular pin fin heat sinks

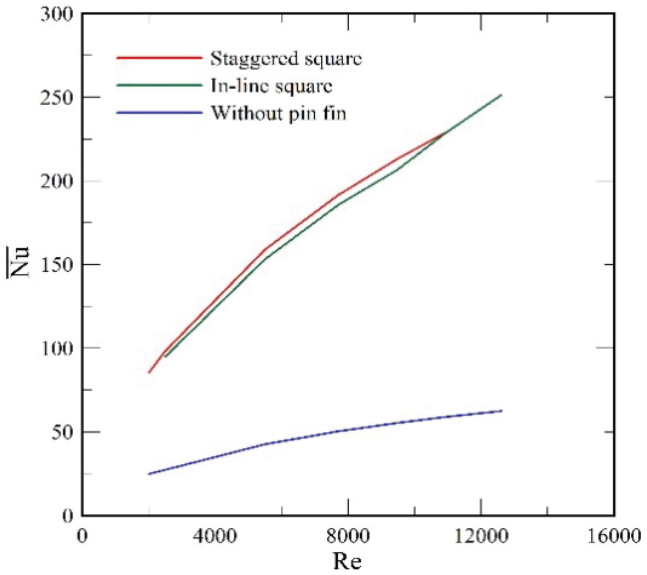

Fig. 5 Variations in average Nusselt number with Re of a square pin fin heat sink

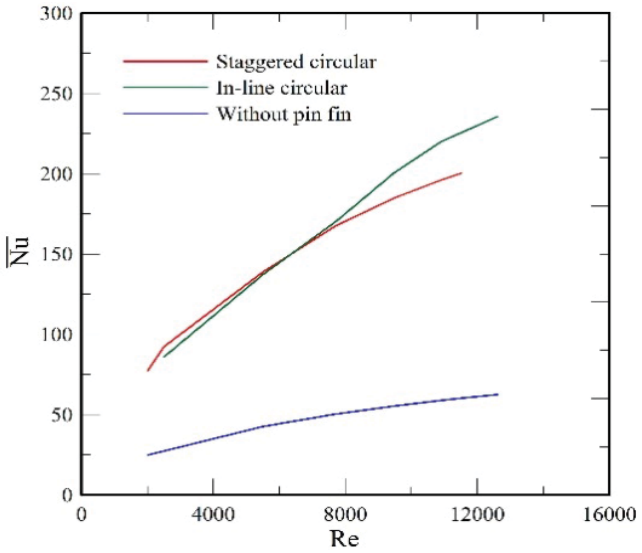

Fig. 6 Variations in average Nusselt number with Re of a circular pin fin heat sink

V. Conclusions

(1) In the present study, the more appropriate turbulence model is the realizable k - ε model to predict the flow fields in the pin fin heat sink channels.
(2) Whether in the staggered or in-line case channel, the stronger fluctuations near the wall of square pin fin channels cause better mixing of fluid and larger thermal boundary layer developing rate in the channel than that of circular pin fin channels.
(3) Whether in square or circular pin fin channel, the stronger fluctuations in the staggered case channels cause larger thermal boundary layer thickness near the downstream of the channel than that of in-line case channels.
(4) In the square pin fin cannel, the average Nusselt number of staggered case channel is slightly higher than that of in-line case channel because of the stronger fluctuations in the staggered case channel cause better mixing of fluids in the channel than that the in-line case channel.
(5) In the circular pin fin channel, the difference of average Nusselt number between the staggered and in-line channels are very close when Re < 8000 and the average Nusselt number of in-line channel are slightly higher than that of staggered case channel when Re > 8000.

Acknowledgment

We really appreciate that the Ministry Science and Technology of Taiwan for supporting this project under contract no. NSC102-2221-E-006-173-MY3.

References

[1] G. Theoclitus, "Heat transfer and flow friction characteristics on nine pin-fin surfaces," *Trans. ASME, J. Heat Transfer*, pp. 383–390, Nov. 1966.
[2] E. M. Sparrow, J. W. Ramsey, "Heat transfer and pressure drop for a staggered wall-attached array of cylinders with tip clearance," *Int. J. Heat Mass Transfer,* vol. 21, pp.1369–1377, 1978.
[3] O. N. Sara, S. Yapici, and M. Yilmaz, "Second law analysis of rectangular channels with square pin-fins," *Int. Commun. Heat Mass Transfer,* vol. 28, no. 5, pp. 617–630, 2001.
[4] G. J. VanFossen, "Heat-transfer coefficients for staggered arrays of short pin fins," *Trans. ASME, J. Heat Transfer*, vol. 104, pp. 268–274, 1982.
[5] D. E. Mezger, C. D. Fan, and S. W. Haley, "Effects of pin shape and array orientation on heat transfer and pressure loss in pin arrays," *Trans. ASME, J. Heat Transfer,* vol. 106, pp. 252–257, 1984.
[6] S. Y. Won, G. I. Mahmood, and P. M. Ligrani, "Spatially-resolved heat transfer and flow structure in a rectangular channel with pin fins," *Int. J. Heat Mass Transfer*, vol.47, pp. 1731–1743, 2004.
[7] F. E. Ames, L. A. Dvorak, and M. J. Morrow, "Turbulent augmentation of internal convection over pins in staggered-pin fin arrays," *Trans. ASME, Journal of Turbomachinery*, vol. 127, pp. 183–190, 2005.
[8] M. E. Lyall, A. A. Thrift, K. A. Thole, and A. Kohli, "Heat transfer from low aspect ratio pin fins," *Trans. ASME, J. of Turbomachinery*, vol. 133 (011001), 2011.
[9] Y. Kondo, H. Matsushima, and T. Komatsu, "Optimization of pin fin heat sinks for impingement cooling of electronic packages," *Trans. ASME, J. Electron. Packag*., vol. 122, no. 3, pp. 240-246, 2000.
[10] M. B. Dogruoz, M. Urdaneta, and A. Ortega, "Experiments and modeling of the hydraulic resistance and heat transfer of in-line square pin fin heat sinks with top by-pass flow," *Int. J. Heat Mass Transfer,* vol. 48, pp. 5058–5071, 2005.
[11] W. A. Khan, M. Yovanovich, and J. Culham, "Optimization of microchannel heat sinks using entropy generation minimization method," In: Semiconductor thermal measurement and management symposium, *2006 IEEE twenty-second annual,* pp.78–86.
[12] M. Shaeri, and M. Yaghoubi, "Thermal enhancement from heat sinks by using perforated fins," *Energy Convers Manag*, vol. 50, pp.1264–1270, 2009.
[13] A. Kosar, and Y. Peles, "Micro scale pin-fin heat sinks-parametric performance evaluation study," *IEEE Transactions on components, packaging and manufacturing technology*, vol. 30, pp. 855–865, 2007.
[14] T. J. John, B. Mathew, and H. Hegab, "Parametric study on the combined thermal and hydraulic performance of single phase micro pin-fin heat sinks Part I: Square and Circle Geometries," *Int. J. of Thermal Sciences,* vol. 49, pp. 2177–2190, 2010.
[15] J. F. Tullius, T. K. Tullius, and Y. Bayazitoglu, "Optimization of microstructured fins in minichannels," *Proceedings of TMNN-2011/068*, Antalya, Turkey, 2011.
[16] J. F. Tullius, T. K. Tullius, and Y. Bayazitoglu, "Optimization of short micro pin-fins in minichannels," *Int. J. Heat Mass Transfer*, vol. 55, pp. 3921–3932, 2012.
[17] Izci Türker, Koz Mustafa, and Ali Kosar, "The effect of micro pin-fin shape on thermal and hydraulic performance of micro pin-fin heat sinks," *Heat Transfer Engineering*, vol. 36, pp. 1447–1457, 2015.
[18] M. L. Elsayed, O. Mesalhy, "Studying the performance of solid/perforated pin-fin heat sinks using entropy generation minimization," *Heat Mass Transfer*, vol. 51, pp. 691–702, 2015.
[19] G. Xie, Y. Song, M. Asadi, and G. Lorenzini, "Optimization of pin-fins for a heat exchanger by entropy generation minimization and constructal law," *Trans. ASME, J. Heat Transfer,* vol. 137, 061901, 2015.
[20] K. Horiuchi, A. Nishihara, and K. Sugimura, "Multi-objective optimization of water-cooled pin fin heat sinks," *Int. J. Heat Mass Transfer*, vol. 81, pp. 760-766, 2015.
[21] H. Jonsson and B. Moshfegf, "Modeling of the thermal and hydraulic performance of plate fin, strip fin, and pin fin heat sinks-influence of flow bypass," *Trans. on components and packaging technologies,* vol. 24, pp. 142-149, 2001.

Yue-Tzu Yang is a Professor at the Department of Mechanical Engineering, National Cheng Kung University, Taiwan. She received her Ph.D. in mechanical engineering from the University of Liverpool, UK in 1990. Her research interests include numerical simulations of turbulent flow, heat transfer enhancement, and electronic cooling.